# Error-related Persistence of Motor Activity in Resting-state Networks

**Nicolò F. Bernardi[1], Floris T. Van Vugt[1,2], Ricardo Ruy Valle-Mena[1,2], Shahabeddin Vahdat[3], and David J. Ostry[1,2]**

## Abstract

■ The relationship between neural activation during movement training and the plastic changes that survive beyond movement execution is not well understood. Here we ask whether the changes in resting-state functional connectivity observed following motor learning overlap with the brain networks that track movement error during training. Human participants learned to trace an arched trajectory using a computer mouse in an MRI scanner. Motor performance was quantified on each trial as the maximum distance from the prescribed arc. During learning, two brain networks were observed, one showing increased activations for larger movement error, comprising the cerebellum, parietal, visual, somatosensory, and cortical motor areas, and the other being more activated for movements with lower error, comprising the ventral putamen and the OFC. After learning, changes in brain connectivity at rest were found predominantly in areas that had shown increased activation for larger error during task, specifically the cerebellum and its connections with motor, visual, and somatosensory cortex. The findings indicate that, although both errors and accurate movements are important during the active stage of motor learning, the changes in brain activity observed at rest primarily reflect networks that process errors. This suggests that error-related networks are represented in the initial stages of motor memory formation. ■

## INTRODUCTION

Learning a motor skill such as playing tennis results in more accurate and faster execution of movements. Such improvements in performance are reflected in changes in brain activity during the task (Shmuelof, Yang, Caffo, Mazzoni, & Krakauer, 2014; Della-Maggiore & McIntosh, 2005; Doyon et al., 2002). However, for learning to persist after training, the brain has to be able to maintain key elements of this newly learned state in the absence of movement. Here we investigate which aspects of the neural state formed during learning persist in the resting periods following motor training.

Recent studies have shown that patterns of brain connectivity at rest are changed following a period of motor learning (Philip & Frey, 2016; Sidarta, Vahdat, Bernardi, & Ostry, 2016; Albert, Robertson, & Miall, 2009). Further studies have shown that the pattern of connectivity in the resting brain is directly influenced by the nature of the task previously performed (Vahdat, Darainy, Milner, & Ostry, 2011; Lewis, Baldassarre, Committeri, Romani, & Corbetta, 2009). Presumably, part of the changes observed in the brain during the task reflects the ongoing formation of new motor memories (Debas et al., 2010) in the form of a progressive brain connectivity rearrangement. These changes not only enable a more efficient execution of the ongoing motor task but also provide the foundation for an increased capacity to perform the task in the future, as revealed by phenomena such as off-line memory consolidation (Brashers-Krug, Shadmehr, & Bizzi, 1996), faster relearning (Huang, Haith, Mazzoni, & Krakauer, 2011), and off-line gains in motor performance (Gregory et al., 2014).

However, the source of the changes in the resting brain following motor learning is unknown. Are the plastic changes observable at rest a reflection of the networks utilized to perform the motor task? Or do they involve different brain areas than those activated during the task? Furthermore, which subcomponents of the network involved in performing and learning the task show evidence of plasticity that persists following learning?

In this study, we hypothesize that changes in brain activation at rest will be observed in areas where activation during the task scales with the quality of motor performance. This could be observed in two ways. It is known that the feedback related to movement error and the feedback related to movement accuracy both provide important contributions when developing a new motor skill (Haith & Krakauer, 2013). When an error is identified, for example, through vision or proprioception, certain brain areas become active to update the motor commands for

[1]McGill University, [2]Haskins Laboratories, New Haven, CT, [3]Stanford University School of Medicine



Journal of Cognitive Neuroscience 30:12, pp. 1883–1901
doi:10.1162/jocn_a_01323

future actions (Wolpert, Diedrichsen, & Flanagan, 2011; Diedrichsen, Hashambhoy, Rane, & Shadmehr, 2005). The pattern of activity and anatomical connectivity of the cerebellum, in particular, has led to the idea that this area contributes to motor learning by comparing the predicted with the actual sensorimotor consequences of a movement (Criscimagna-Hemminger, Bastian, & Shadmehr, 2010; Miall & Wolpert, 1996). On the other hand, other brain areas that participate in motor learning have been shown to become more active when movement errors are low, that is, when accuracy is high. Areas of the BG in particular, such as the ventral putamen, have been shown to be active for successful motor performance (Widmer, Ziegler, Held, Luft, & Lutz, 2016; Lutz, Pedroni, Nadig, Luechinger, & Jäncke, 2012; Schultz, 1998) and to become deactivated in proportion to error magnitude (O'Doherty, Dayan, Friston, Critchley, & Dolan, 2003). These previous studies suggest that the brain utilizes information pertaining to the quality of movement at both ends of the performance spectrum, in particular, that some areas show increased activity with larger errors and other areas show decreased activity with larger errors. Here we ask whether these two types of brain responses provide the basis for the changes in resting-state functional connectivity (RS-FC) observed after task completion. Specifically, we ask whether the changes in the patterns of brain activity that persist following learning are primarily forged from the movements that were more accurate, from those that were less accurate, or from both.

In this study, we aimed to characterize the spontaneous brain activity following learning of a motor task using fMRI. Participants learned to trace an arc-shaped trajectory with fast and accurate movements. The precision of motor performance was quantified along a unidimensional continuum, in terms of spatial distance from the arc, with greater distance indicating poorer performance and smaller distance indicating better performance (i.e., more accurate arc tracing). We used the brain imaging data collected while participants performed the task to search for areas in which the amount of activation scaled positively or negatively with the spatial error (distance from the arc). Areas showing increased activations for trials in which the movement trace was closer to the target arc were interpreted as areas tracking movement accuracy. Areas showing increased activation for trials with greater mismatch from the prescribed arc were interpreted as tracking movement error. We then examined whether changes in RS-FC observed after the training overlapped either or both of these networks.

## METHODS

### Participants

A total of 20 right-handed participants were recruited (nine women, mean age = 24.8 years, *SD* = 5.3 years) and provided written informed consent. The participants were healthy adults with no physical or neurological conditions. All procedures were approved by the research ethics board at the Institut Universitaire de Gériatrie de Montréal, Montreal, Quebec, Canada (CMER RNQ 12-13-023). The experimental session for each participant lasted 2.5 hr overall.

### Behavioral Task

The behavioral paradigm in this study was based on the task developed by Shmuelof et al. (Shmuelof et al., 2014; Shmuelof, Krakauer, & Mazzoni, 2012), with various changes to suit the specific needs of the current study. While lying down inside the MRI scanner, participants had to trace a thin arc-shaped trajectory quickly and accurately, using a fiber-optic fMRI-compatible computer mouse (NAtA Technologies, FOM-2B-10B). Participants rested their arms on a custom-made Plexiglas fMRI-compatible adjustable table (Hybex Innovations;

**Figure 1.** Design of the experiment. (A) Picture of the MRI-compatible adjustable table, over which participants held the computer mouse for the task. (B) Visual display as seen by participants during the task-based part of the experiment. At the appearance of the black dot, participants had to quickly and accurately retrace the thin white arched trajectory, landing into the target circle. While doing so, participants were shown the trajectory generated thus far as a gray trace. At movement completion, the entire trajectory remained visible on screen for 1.5 sec and, together with the target circle, changed color to provide feedback about movement duration (green = correct duration, red = too fast, blue = too slow). (C) Sequence of the experimental tasks. The experiment began with 20 warm-up trials on a straight-path task to familiarize participants with the mouse, followed by the pretraining resting-state scans. After two familiarization trials with the arc-tracing task, participants started the motor training part of the experiment, comprising 180 trials, subdivided in three runs of 60 trials each with breaks in between. Each run comprised six blocks of task (shown as purple rectangles) and six blocks of rest (shown as cyan rectangles) presented in alternation. Continuous fMRI recordings were performed during each run. Following motor training, participants underwent the posttraining resting-state scans. (D) Details of the task-based fMRI design. The gray solid vertical lines indicate the beginning of each trial. The green dotted lines show the occurrence of each TR in the fMRI sequence. The brown boxcar functions represent the time course and weight for the three regressors employed in the fMRI analysis. The Movement regressor was a binary function based on the exact onset and duration of each motor movement. The intermovement regressor was complementary to the movement regressor, thus capturing the epochs within a task block when participants were not moving. The behavioral modulation was a graded function containing the distance from the arc, peak velocity, movement duration, or path length on each trial. Four different behavioral regressors were used in the analysis, one for each of the four behavioral variables. (E) Orthogonalizations. Each of the four behavioral modulation regressors was orthogonalized with respect to the movement and intermovement regressors, thus capturing the brain activation correlated with specific features of motor performance, such as the distance from the arc, after taking into account the variations in the BOLD signal due to simply executing the movements and preparing for the subsequent movement. Peak velocity, movement duration, and path length are grayed out to indicate that they were included in the analyses as control variables, whereas the distance from the arc was the main variable of interest.

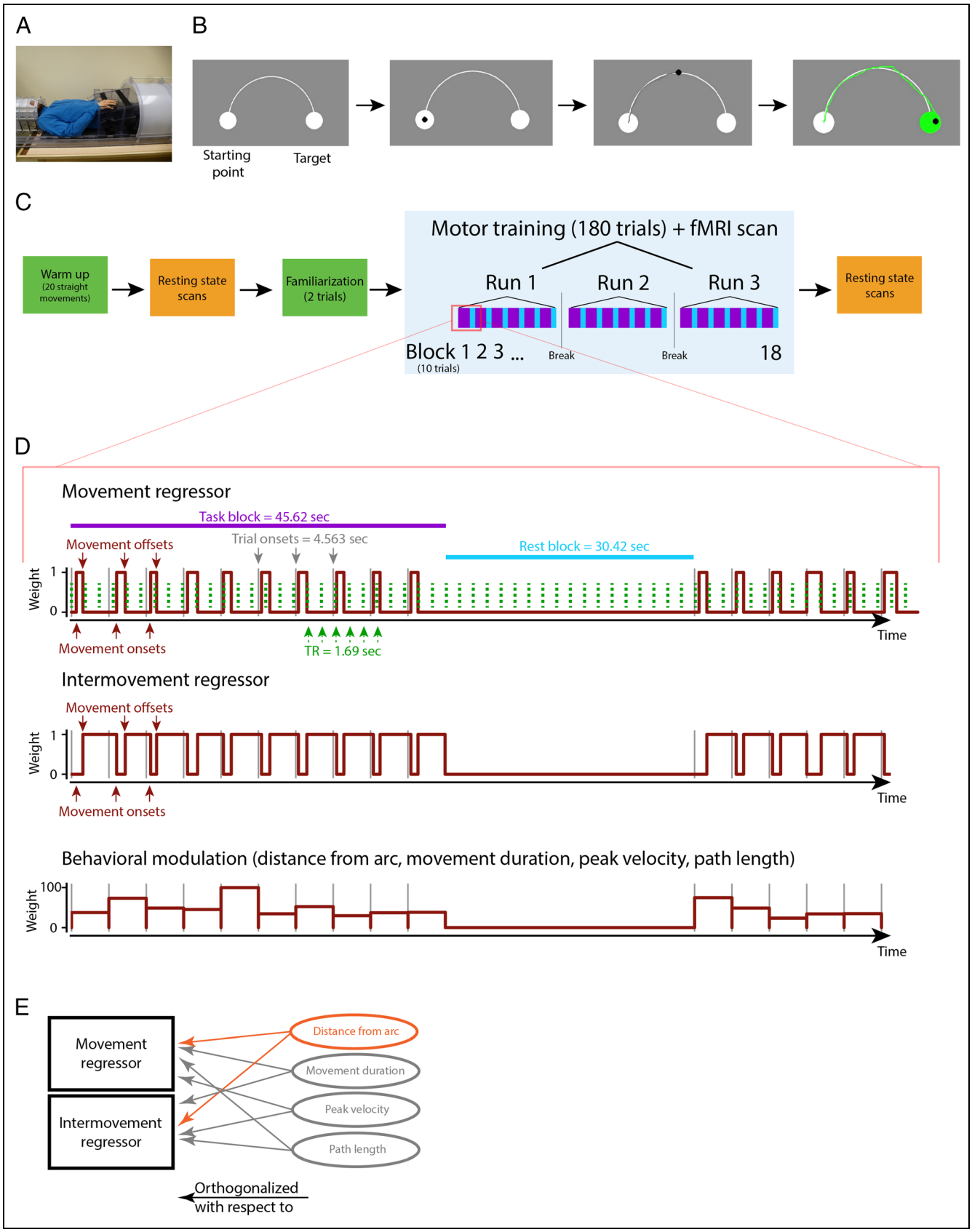
A
B
Starting point
Target
C
Warm up (20 straight movements)
Resting state scans
Familiarization (2 trials)
Motor training (180 trials) + fMRI scan
Run 1
Run 2
Run 3
Block 1 2 3 ...
(10 trials)
Break
Break
18
Resting state scans
D
Movement regressor
Task block = 45.62 sec
Movement offsets
Trial onsets = 4.563 sec
Rest block = 30.42 sec
Weight
1
0
Movement onsets
TR = 1.69 sec
Time
Intermovement regressor
Movement offsets
Weight
1
0
Movement onsets
Time
Behavioral modulation (distance from arc, movement duration, peak velocity, path length)
Weight
100
0
Time
E
Movement regressor
Intermovement regressor
Distance from arc
Movement duration
Peak velocity
Path length
Orthogonalized with respect to

Figure 1A) that enabled them to comfortably rest their arm and hold the computer mouse while minimizing movements at the elbow and minimizing the flexion of the wrist. On the monitor inside the MRI, participants were shown a starting circle, a target circle, and a connecting arc (Figure 1B, first panel). The width of the arc on screen was 8.82 cm. At the onset of each new trial, a black cursor dot appeared in the starting circle (Figure 1B, second panel), which signaled participants that they could start their movement. The cursor radius on screen was 4.7 mm. For the purpose of providing a duration feedback during the experiment, movement initiation was determined as the first moment participants were farther than 8.43 pixels (0.50 cm) away from the starting point. Movement initiation was not under time pressure, that is, the task was not meant to gauge RTs. Participants were required to retrace the arc shape shown on the screen as accurately as possible. Real-time visual feedback of motor performance was provided to participants by both the moving black cursor dot as well as by a trace showing the trajectory generated so far (Figure 1B, third panel). A movement was considered completed when the cursor dot reached the target circle and remained in it for at least 150 msec. When the movement was completed, the traced trajectory and the target circle changed color, indicating whether the movement duration was in the desired range (Figure 1B, fourth panel). Blue indicated that the movement had been performed too slowly (>1000 msec), red indicated that the movement had been performed too quickly (<800 msec), and green indicated that the movement duration was correct. Participants were asked to maintain their speed in the desired range. Thus, the task instructions emphasized learning in the spatial domain while constraining movement duration to remain the same throughout the training. The movement trace remained on the screen for an additional 1.5 sec following movement completion, thus providing participants with off-line visual feedback about their overall performance. To prevent participants from having to return to the starting position after completing a trial, the location of the starting and target circle was swapped between trials. On odd trials, the starting circle was on the left and participants had to move toward the right, whereas on even trials the starting circle was on the right and participants had to move toward the left. Figure 1C depicts the sequence of the experimental tasks. The experiment began with 20 warm-up trials, during which participants performed straight point-to-point reaching movements using the computer mouse in the scanner. No brain scans were acquired in this first part, the purpose of which was to familiarize participants with the equipment (mouse, monitor, adjustable table) and to maximize the chances to observe intrinsic brain activity in the motor networks in the subsequent resting-state scans. The warm-up trials were followed by two pretraining resting-state scans, followed by the motor training, followed by two posttraining resting-state scans. The motor training comprised a total of 180 trials, subdivided into three runs of 60 trials each. Each run consisted of six blocks, each containing 10 consecutive trials, with a new trial starting every 4.563 sec. This duration was chosen to accommodate even the slowest movements, as assessed during pilot experiments, and also to be a multiple of the repetition time (TR; see Brain-imaging Procedures section). If a participant failed to enter the target area within 4.563 sec from the onset of the trial, the trial was interrupted without providing a duration-based feedback, and a new trial was automatically started. These trials were not removed from further analyses. Between movement blocks, participants remained still with their eyes open to allow recording of their brain activity at rest. Participants were given a 5-min break between each run, during which they were allowed to close their eyes while remaining in the MRI scanner. Immediately before the beginning of the training, participants performed two familiarization trials, one in each direction. The familiarization trials were included to ensure that participants were performing the task according to the instructions and to give them the chance to ask questions before the beginning of the motor training.

### Behavioral Data Analysis

During training, samples were acquired from the computer mouse on an event-related basis, using the Human Interface Device protocol over USB. As a result, there was no fixed sampling rate, and the rate of incoming events depended on the amount of movement. With our hardware, maximum event rates were at about 8-msec intervals (125 Hz).

The data acquired from the computer mouse were resampled off-line at 1000 Hz and filtered using a Butterworth low-pass filter (cutoff: 10 Hz). For the purpose of the kinematic analyses, the beginning of a movement was defined as the frame at which velocity exceeded 5% of peak velocity. The end of a movement was defined as the frame at which the cursor entered the target area (provided that after entering the target area the cursor remained there until trial completion). For each trial, we quantified motor performance as the maximum absolute perpendicular distance between the 2-D trajectory of the movement and the coordinates of the reference arc. Thus, a larger distance from the arc indicated greater movement error. In the subsequent neuroimaging analyses, the behavioral error score was used to identify the brain areas showing an increase in activation in proportion to the amount of error (see Task-based Activations section). Measures of distance from the arc were computed on spatially normalized kinematic traces to prevent movement velocity from biasing the distance estimates.

In addition to the distance from the arc, we also computed possible confounding kinematic variables, such as movement peak velocity, movement duration, and path length, so that we could control for them by including them

as covariates in the neuroimaging analyses (see below). A small percentage (2.2%) of trials were affected by either imperfect responses of the mouse device, evidenced by the cursor failing to respond to the participant's movements or by participants' aberrant behaviors, such as moving in the wrong direction. These trials were marked as outliers, and their kinematic outcomes were not used in further analyses. Kinematic data were averaged for each participant within each block of 10 trials. The difference in movement error between the first and last block of training was utilized as a measure of motor learning: Motor Learning (ML) = Average (Max Abs Distance)$_{BLOCK1}$ − Average (Max Abs Distance)$_{BLOCK18}$ (see Figure 2C later in this paper).

### Brain-imaging Procedures

MRI data were acquired using a 3.0-T MRI scanner (Tim Trio, Siemens). The experiment began with two pretraining resting-state runs, followed by three task-based runs, followed by two posttraining resting-state runs (Figure 1C). During resting-state scans, participants were instructed to lie quietly with their eyes closed and avoid any head motion during the scan. We acquired two separate but consecutive resting-state scans, rather than a single continuous scan, to prevent participants from falling asleep. The task-based scanning was broken into three runs to allow participants to rest throughout the motor training. To reduce head motion and scanner noise, foam padding and earplugs were provided to the participants. Functional images were obtained using the Simultaneous Multi-Slice BOLD-EPI WIP sequence (Setsompop et al., 2012) as follows: slice acceleration factor = 3; TR = 1690 msec; echo time = 30 msec; in-plane resolution = 2 × 2 mm$^2$, slices = 63; thickness = 2 mm (no gap); field of view = 200 mm × 200 mm; and flip angle = 60°. We collected 250 volumes for each resting-state run (about 7 min) and 273 volumes for each task-based run (about 7.7 min). Each of the three task-based runs comprised six task blocks and six rest blocks presented in alternation (Figure 1C). The first task block was preceded by three volumes of rest ($t$ = 5.07 sec, not shown in the figure), which were subsequently discarded (see fMRI Data Analysis). Each task block lasted 45.62 sec (27 volumes, 10 movement trials), so that the end of the 10th movement trial in each block would coincide with the first TR of a resting block (Figure 1D). Each rest block lasted 30.42 sec (18 volumes). Thus, we collected a total of 162 task and 108 rest volumes in each run and 486 task and 324 rest volumes throughout the whole task-based scanning procedure. We used a multiband accelerated imaging sequence in the functional sequences of the current study because it enabled acquisition of more data in a relatively short scan time (Moeller et al., 2010). Simultaneous acquisition was achieved using a 32-channel multiarray head coil. Structural images were acquired with a T1-weighted 3-D multi-echo MPRAGE sequence as follows: TR = 2530 msec; slices = 176; thickness = 1 mm (no gap); flip angle = 7°; and field of view = 256 mm × 256 mm, iPAT mode = ON (GRAPPA, Acceleration 2).

### fMRI Data Preprocessing

Data preprocessing was performed using FMRIB software library (FSL) Version 5.0.9 (www.fmrib.ox.ac.uk, FMRIB; Smith et al., 2004). For both the task-based and resting-state scans, image preprocessing consisted of the following: the removal of the first three volumes in each scan (volumes acquired before equilibrium magnetization was reached), nonbrain removal using Brain Extraction Tool, motion correction (using a six-parameter affine transformation implemented in the FMRIB Linear Image Registration Tool), spatial smoothing with a 5-mm FWHM Gaussian kernel, and temporal high-pass filtering (Gaussian-weighted least-squares straight line fitting, σ = 100.0 sec). A boundary-based registration with field map correction was utilized to align the participant's functional image to the participant's structural space (Greve & Fischl, 2009). Nonlinear registration using the FMRIB Nonlinear Image Registration Tool was used to normalize the structural space to the standard MNI152 template. For the purpose of physiological noise removal, in both the task-based and resting-state scans, we computed the average signals taken over white matter (WM) and cerebrospinal fluid (CSF), and we used the resulting time series as nuisance regressors (Shehzad et al., 2009) in the subsequent multiple regression analyses. To extract the WM and CSF time series, we segmented each individual's high-resolution structural T1 image using an automatic segmentation program implemented in FSL. The resulting segmented WM and CSF images were then thresholded to ensure 90% tissue type probability. Each thresholded mask was then applied to that individual's time series, and the mean time series was calculated by averaging the time series from all voxels within the mask. Six additional nuisance regressors were included in both the task-based and resting-state analyses, corresponding to the 3-D translation and rotation estimated during registration (Friston et al., 1995). For both the task-based and resting-state analyses, we also identified time points in the fMRI data set suspect to have been corrupted by large head motion. Using the *motion_outlier* routine within FSL, we generated for each task or resting-state run a confound matrix that was subsequently used in a general linear model (GLM) to completely remove the effects of these time points on the analysis. As per the FSL default, the threshold used to define an outlier was the 75th percentile + 1.5 times the interquartile range of the root mean square intensity difference of volume $N$ to the reference volume (3.9% of the total volumes collected during the task and 3.0% of the total volumes collected during the resting-state were discarded in this way). For the resting-state data only, we performed an

additional step to identify further noise artifacts by means of independent component analysis (ICA), as implemented in the Multivariate Exploratory Linear Optimized Decomposition into Independent Components within FSL. Several options have been developed to isolate the noise components from the independent components identified in resting-state data. Automated procedures exist, such as AROMA (Pruim et al., 2015), which has been shown to effectively remove noise related to head motion. However, this procedure does not take into account the noise due to physiological signals such as heart rate and respiration. When taking into account both physiological and head motion-related noise, the consensus is that visual inspection of the components represents the gold standard for component classification (Griffanti et al., 2017). There is presently no consensus on the optimal number of components for noise removal. For our present application, the ICA dimension was determined automatically by the software. The total number of in- dependent components ranged from 45 to 60. From this, components associated with cardiorespiratory noise, signal dropout, and sudden head motions were identified by visual inspection following the guidelines by Kelly et al. (2010). For each participant, up to a maximum of 20% of the total number of independent components were labeled as noise. The time series for these components were computed on a per-participant basis and added as a nuisance component in the subsequent multiple regression analyses.

### Task-based Activations

Participant-level statistical analyses of the movement task were performed using the fMRI Expert Analysis Tool (FEAT) toolbox in FSL. Brain responses for each run of each participant were modeled separately. For each run, we modeled brain responses using six regressors. The first regressor was constructed from a boxcar function representing the precise onset and duration of each movement (Figure 1D, top row), convolved with a gamma-based hemodynamic response function (HRF). This regressor was designed to capture the brain activations related to producing the actual movement. The second regressor, which we called "intermovement," was constructed based on the precise onset and duration for each of the brief (~3.5 sec) resting epochs interspersed between two adjacent movements (Figure 1D, middle row). The onset and offset of each resting epoch coincided with the end of the previous movement and the beginning of the next movement, respectively. The second regressor was also convolved with a gamma-based HRF. This regressor was designed to capture the brain activations related to the nonexecution components of the task, such as processing the feedback from the immediately preceding movement and planning for the following movement. Note that each trial had a different movement and intermovement duration, depending on participants' behavior on each trial, causing the two regressors to be inherently jittered in time. The statistical maps generated by these two regressors revealed the brain areas responsive to the contrast of task (subdivided into its movement and intermovement components) versus rest. The subdivision of the design into movement and intermovement regressors was preferred to the use of a single continuous regressor because it does not carry the assumption that a given brain area would be engaged throughout the entire time of a trial. Instead, each regressor is capable of capturing activations that might be temporally limited to the motor epochs of a trial (movement regressor) or to the nonmotor epochs (intermovement regressor), with activations that are common to both epochs appearing in both regressors. Figures 3 and 4 show that the maps for the movement and intermovement regressors were indeed different from each other, indicating that brain activity differed between these epochs. In the analyses that follow, unless explicitly stated, we have focused on the movement regressor, given that relatively little activation is seen in the intermovement period.

### Task-based Behavioral Modulation

The main purpose for collecting task-based activations in this study was to identify areas in the brain in which activation scaled with the quality of motor performance. Therefore, a third regressor in the task-based GLM was included to investigate changes in the brain specifically attributable to the amount of spatial error on a trial-by-trial basis (Figure 1D, third row). This time series encoded the distance from the arc for each trial and was orthogonalized, after convolution with the HRF, with respect to the first two predictors, that is, the main effect of task versus rest (Figure 1E). Therefore, this regressor was designed to detect activations in the brain related to the behavioral modulation—in this case, the distance from the arc. As a result of this procedure, the behavioral modulation maps reflected neural activations specifically related to the magnitude of movement error and were not confounded by activation attributable to motor execution. On the other hand, the behavioral modulation maps were not indicative of motor learning over the course of the entire training procedure, as the modeling of error was done on a per-run basis. It was additionally assumed that movement error could play a role in modulating both the brain responses during movement execution as well as during the intermovement epochs. Therefore, a single behavioral modulation regressor was included in the model; this regressor had the duration of an entire trial as per the experimental design (4.563 sec), and its onset time was the beginning of each trial, as marked by the appearance of the black cursor on the screen (Figure 1D, third row).

As a result of this design, we were able to identify the areas in the brain that showed greater activity in proportion to increasing movement error and, separately, areas that showed greater activity in proportion to decreasing movement error, that is, increasing movement accuracy.

Thus, a positive behavioral modulation map contained areas showing increased activation in trials with greater distance from the arc (i.e., greater error), and a negative behavioral modulation map contained areas showing increased activation in trials with less distance (i.e., greater accuracy). Note that the negative behavioral modulation map is not what in the neuroimaging literature is referred to as a task-negative map. Whereas the negative behavioral modulation map in our study refers to the areas of the brain showing increased activation for trials with lower distance from the arc, the task-negative map refers to the areas of the brain showing greater activation during rest compared with task, which is not the focus of the present investigation.

After this analysis was completed for each run of each participant separately, a group-level mixed-effects model analysis (FLAME 1) was performed using the same toolbox. In the group analysis, each participant contributed three inputs, one for each run. Because we were interested in error-related areas at any time during learning, the three runs were combined by means of an $F$ test, the results of which show the areas where activity in any of them (or any combination of them) was significantly different from zero. For this group analysis, corrections for multiple comparisons at the cluster level were performed using Gaussian random field theory (minimum $z = 3.5$; cluster significance, $p < .05$, corrected).

### Additional Control Variables

It is known that movement error may correlate, at the behavioral level, with other dimensions of motor performance, such as movement velocity (Fitts, 1954). The correlation of error with other aspects of motor execution creates a potential source of ambiguity in the interpretation of the positive and negative behavioral modulation maps, as these maps may reflect to various degrees the contribution of responses unrelated to the amount of error. To address this potential problem, we included in the model described above three additional behavioral regressors known from other motor tasks to bear a relationship with movement error, namely, movement duration, movement peak velocity, and path length. Each of these regressors was orthogonalized, after convolution with the HRF, with respect to the first two regressors, that is, the main effect of task versus rest (Figure 1E). By including movement error (i.e., the distance from the center of the arc), movement duration, peak velocity, and path length in the same GLM, we sought to identify brain regions that showed error-related responses after having taken into account the potential contribution to the variability in the BOLD signal due to the three other behavioral regressors. Two variations of this analysis were run, in which the movement error regressor had been orthogonalized with respect to movement duration, velocity, and path length. In one analysis, the HRF-convolved time series of duration, velocity, and path length were regressed out from the HRF-convolved time series of movement error, which was then entered as the only behavioral regressor in the GLM. In another analysis, all four behavioral regressors were entered in the GLM, and the movement error regressor was orthogonalized with respect to the three other behavioral regressors. These two analyses generated results highly similar to the original analysis and, therefore, are not reported here.

### ROI Identification

Analysis of the RS-FC was performed using a seed-based whole-brain correlation analysis. The list of seeds used in this study with their corresponding MNI coordinates and the associated $Z$ value can be found in Table 1. We

**Table 1.** List of ROIs Used in the Resting-state Analyses

| *Seed* | *Anatomical Label* | *Z Score* | *x* | *y* | *z* |
|---|---|---|---|---|---|
| *From the Movement Map* | | | | | |
| M1/S1 | Left primary sensorimotor cortex | 7.0 | −32 | −30 | 68 |
| PMd | Left dorsal premotor cortex | 6.6 | −26 | −22 | 66 |
| CB-VI | Right cerebellar lobule VI | 4.1 | 16 | −62 | −26 |
| CB-VIII | Right cerebellar lobule VIII | 5.9 | 26 | −52 | −52 |
| vPut | Left ventral putamen | 5.2 | −16 | 14 | −8 |
| *From the Intermovement Map* | | | | | |
| OFC | Left orbitofrontal cortex | 4.0 | −40 | 44 | −16 |

The coordinates are according to the MNI standard template. $Z$ values indicate the local maxima at the ROI center obtained from the group movement or intermovement positive maps.

defined six seeds, or ROIs, based on the activation foci at the group level from the task-positive map (during movement or intermovement positive epochs). All seeds were lateralized in the left hemisphere to reflect the fact that the motor task was performed with the right hand. The seeds were chosen from the task-based maps to ensure that the ROIs were functionally relevant, that is, involved in performing the motor task. The purpose of the study was to investigate the persistence of error-related task-based networks in subsequent resting-state periods. Using task-based areas as probes increased the likelihood that the networks observed in the resting state were indeed involved in performing the task. Two seeds were chosen in areas known to be activated in response to movements performed with high error: the cerebellar lobule VI (right CB-VI) and the cerebellar lobule VIII (right CB-VIII) (Diedrichsen et al., 2005). Two seeds were chosen in areas known to be activated in response to movements performed with low error (i.e., high accuracy), the ventral putamen (left putamen), and the OFC (left OFC) (Howard, Gottfried, Tobler, & Kahnt, 2015; Wickens, Reynolds, & Hyland, 2003). Two additional seeds were chosen in areas known to play an important role in motor learning in general: the primary sensorimotor cortex (left M1/S1) and the dorsal premotor cortex (left PMd). The seeds were defined to jointly maximize the $z$ scores from the task-positive map and the probability of being in the chosen anatomical ROI as defined by the Juelich histological atlas for the cortical seeds (Eickhoff et al., 2005) and by the probabilistic cerebellar atlas for the cerebellar seeds (Diedrichsen, Balsters, Flavell, Cussans, & Ramnani, 2009). Each ROI was represented as a spherical mask of 6-mm radius.

### RS-FC with Behavioral Factors

We estimated the correlation between the BOLD signal in the seed region and every other voxel in the brain by means of multiple regression analysis in FSL's FEAT. The ROI's mean time series was the main predictor of interest, and a number of nuisance regressors were included: the average time series of WM, CSF, the noise components obtained from ICA, the six motion parameters, and the motion outlier confound matrices. The results were brain regions that were temporally correlated with the seed after accounting for unwanted temporal noise. These steps were repeated for all seeds on every run of each participant. The results of this low-level analysis were submitted to a group-level mixed-effect model analysis (FLAME 1), aimed at contrasting the functional connectivity in the two pretraining resting-state runs with the two posttraining runs. The Motor Learning score was used here to obtain a weighted average of the difference between scans (Pretraining compared with Posttraining) as explained previously (Vahdat et al., 2011). As contrast of interest in the GLM, instead of an unweighted regressor that was $-1$ for prescans and $+1$ for postscans, we used a regressor weighted by the participant's individual motor learning score, say $x$, so that the regressor was $-x$ for pretraining scans and $+x$ for posttraining scans. For each cluster in which a significant Post $-$ Pre difference was found, we examined the correlation between the behavioral measure (Motor Learning) and changes in functional connectivity from pre- to posttraining resting-state scans at the group level. In this study, we report only those clusters whose change in activity was reliably correlated with behavior (see scatterplots in Figure 5). Furthermore, for each cluster that showed a significant correlation with behavior, we compared the pretraining and posttraining functional connectivity, averaged within the cluster (see bar plots in Figure 5). This comparison was run for each cluster by means of a dependent samples $t$ test. Clusters within which functional connectivity was not significantly different from zero at the group level in both the pre- and posttraining, as assessed by a $t$ test relative to 0 (alpha level = .05), were discarded. Clusters in the group maps were corrected using a Gaussian random field theory procedure, as implemented in FSL (minimum $z$ = 2.4). Three levels of corrections for multiple comparisons were utilized for the resting-state analyses. First, the cluster significance $p$ value was itself corrected using Bonferroni correction to take into account the fact that six independent group analyses were run, one for each seed. The $p$ value for cluster significance was therefore set as $p$: .05/6 = .0083. Second and third, the $p$ value to assess a significant correlation with behavior, as well as the $p$ value to assess a significant change from pre- to posttraining in functional connectivity scores (Figure 5, two rightmost columns), were set as $p$ = .05/6 = .0083.

### Conjunction Analyses

A first set of conjunction analyses was run to determine whether the areas showing behavioral modulation overlapped the areas involved in performing the task. Thus, rather than considering all the areas with error-related responses, we restricted the analyses to the areas that were also reliably more activated during task compared with rest (i.e., the task-positive map). The conjunction analysis with the task-positive map was performed for both the areas showing positive behavioral modulation as well as for those showing negative behavioral modulation.

A second set of conjunction analyses was run to determine whether the maps showing learning-related changes in RS-FC overlapped the behaviorally modulated positive or negative maps, the former showing the areas with greater response for greater distance from the arc (i.e., greater movement error) and the latter representing the areas showing greater responses for lower distance from the arc (i.e., greater movement accuracy). For the behavioral modulation maps in the latter conjunction analysis, we used the output of the first conjunction analysis, that is, the portions of the behavioral

modulation maps that overlapped the task-positive map. Similar conjunction analyses between task-based modulation maps and RS-FC maps were also run for the movement duration, peak velocity, and path length-modulated maps to establish the potential contribution of these additional variables to posttraining RS-FC. All conjunction analyses were performed using the *easythresh_conj* script (provided by https://www2.warwick.ac.uk/fac/sci/statistics/staff/academic-research/nichols/scripts/fsl/easythresh_conj.sh).

## RESULTS

### Behavioral Performance

Figure 2 depicts movement trajectories at the beginning (Figure 2A) and at the end (Figure 2B) of training for a representative participant. In black is shown the prescribed arc trajectory, whereas in color are shown five rightward trajectories generated by the participant during individual blocks of training. It can be seen that, over the course of training, participants improve their ability to trace the prescribed arc, as evidenced by a smaller distance between the actual and the desired trajectory. We expressed motor performance for each trial as the maximum absolute perpendicular distance between the actual and the desired arc trajectory. Figure 2C shows group averages for this motor performance score over the course of the 18 blocks of training. Motor learning was quantified as the difference between motor performance in the first and last block of training. The difference in the maximum distance from the arc between the first and last block of training was on average 16 pixels and was statistically significant (dependent samples $t$ test: $t(19) = 8.8$, $p < .001$). This shows that participants improved their movements, following the prescribed arc more closely at the end of training. These changes were accompanied by a reduction in movement peak velocity as well as a reduction of path length over the course of training (peak velocity Block 1: 1251 pixels/sec; Block 18: 916 pixels/sec; $t(19) = 3.9$, $p = .001$; path length Block 1: 488 pixels; Block 18: 449 pixels; $t(19) = 3.5$, $p = .002$). On the other hand, the improvement in the distance from the arc was achieved without significant changes in overall movement duration, $t(19) = 0.9$, $p > .3$. The average correlation (Pearson correlation coefficient) between movement distance from the arc and the other three movement variables, computed using the 180 trials for each participant and then averaged across participants, was $r = .02$ for movement duration, $r = .35$ for peak velocity, and $r = .21$ for path length. In addition to the improvement in spatial accuracy, participants improved their ability to complete their movement within the prescribed time window. On average, the percentage of trials having the prescribed duration increased from 34% ± 4.5% ($M \pm SE$) in the first block of training to 66% ± 4.2% in the last block, and this increase was statistically significant, $t(19) = -5.36$, $p < .001$. The increase in the percentage of trials having accurate duration was positively correlated with the increase in spatial accuracy (Pearson correlation coefficient: $r(18) = .62$, $p = .004$), indicating that participants who improved the spatial accuracy of their movements also improved their timing.

### Brain Activations Modulated by Behavioral Performance

Figure 3 and Table 2 show the clusters in which brain activity was positively correlated with the distance from the arc on a trial-by-trial basis. Importantly, these activations are identified after removing the average level of activation during task execution, because in the GLM the behavioral modulation regressor has been orthogonalized relative to the regressor for task versus rest epochs. Thus, the activations observed in these areas can be interpreted as related to error magnitude over and

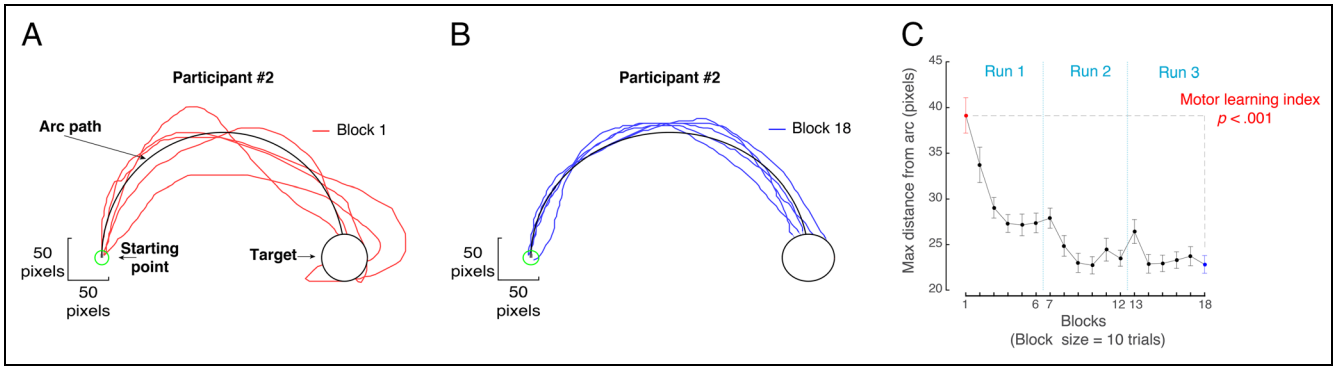


**Figure 2.** Motor learning in the arc-tracing task. (A) The red traces show the five rightward movements in the first block of training for a representative participant. The thick black line indicates the desired arched trajectory, with the empty green and black circles indicating the starting position and the target, respectively. (B) The blue traces show the five rightward movements in the last block of training for the same participant. It can be seen that training results in an increased ability to accurately reproduce the desired arched trajectory. (C) Group-averaged data. The maximum absolute perpendicular distance between the actual and the desired arc trajectory significantly decreases from the first to the last block of training ($p < .001$), indicating motor learning.

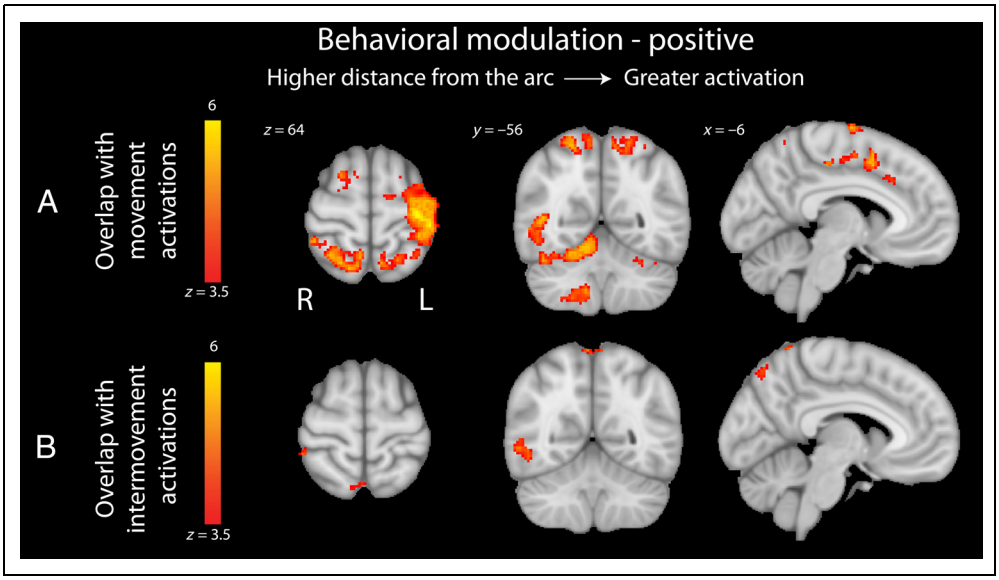


**Figure 3.** Task-based activations related to movement error. Shown are the areas of the brain that were significantly more activated in trials with greater distance from the arc, that is, showing a positive behavior-dependent modulation of the neural responses. The first row shows the results of the conjunction analysis between the positive behavioral modulation map on the one hand and the areas showing increased activations during movement execution (movement regressor) on the other hand. The second row shows the results of the conjunction analysis between the positive behavioral modulation map and the areas showing increased activations during the intermovement epochs (intermovement regressor). Areas showing increased activations for increased distance from the arc included primary motor and somatosensory cortex, dorsal premotor and supplementary motor cortex, the dorsal visual pathway, the superior and inferior parietal lobules, and lobules V, VI and VIII of the cerebellum. R = right hemisphere; L = left hemisphere. The *x*, *y*, and *z* coordinates of cross-sections are reported in MNI space.

beyond their involvement in simply performing the task. Figure 3A shows the error-related activations in areas associated with the active movement periods, whereas Figure 3B gives the map in which activation is associated with periods between movements. It is seen that the most substantial activity related to movement error occurs in conjunction with the movement itself. In this case, a widely distributed network showed increased activation in proportion to the magnitude of the distance from the arc (i.e., in proportion to greater movement error), comprising the cerebellar cortex and vermis, the visual areas along the dorsal pathway, the inferior and superior parietal lobules, primary somatosensory cortex, primary motor cortex, dorsal premotor cortex, SMA, and ACC.

A complementary analysis was undertaken to identify areas that were more active when distance from the arc was less, that is, when motor accuracy was higher, shown in Figure 4. The brain areas showing increased activation for decreased distance from the arc during movement (Figure 4A) or in the intermovement interval (Figure 4B) are also shown under the negative behavioral modulation section of Table 2. These areas comprised the bilateral ventral putamen, the nucleus accumbens, and the left OFC.

## Changes in Functional Connectivity Related to Motor Learning

Figure 5 shows the areas of the brain whose resting-state connectivity changes when learning occurs. It also shows the portion of these resting-state changes that overlap the error-related responses observed during the task (Table 3). The first column of Figure 5 shows the coordinates and location of each seed for which significant changes in RS-FC were detected. The three central columns show the brain areas that increased their functional connectivity with the given seed from pre- to posttraining, with the seed being presented in the first column, in the same row. The green map shows the RS-FC maps, the red map shows the positive behavioral modulation map from the task-based part of the study (i.e., areas showing greater activation for greater distance from the arc), and the yellow overlay shows the overlap between the two. As in Vahdat et al. (2011), we sought to identify changes in RS-FC that were specifically related to motor learning by computing weighted group averages, such that each participant's change in RS-FC was scaled by their amount of motor learning. For each cluster identified in this way, we ran unweighted secondary analyses on the RS-FC data to confirm that (1) a significant change in RS-FC had occurred from pre- to posttraining and (2) the amount of RS-FC change from pre- to posttraining was correlated with the amount of motor learning. The results of these secondary analyses are shown in the last two columns of Figure 5.

It can be seen in Figure 5 that there is a learning-related increase in RS-FC between the lobule VI of the cerebellum and the cortical premotor, primary motor, and primary sensory areas. The strengthening of this connection was apparent in two independent sets of findings. First, it manifested as an increase in RS-FC between the seed in left PMd and lobule VI of the cerebellum on the left side (Figure 5A, first row). Second, it occurred as an increase in RS-FC between the seed in the right CB-VI and a cluster comprising M1, S1, and PMd in the left hemisphere

**Table 2.** Clusters Showing Activation in Proportion to Movement Error

| *Anatomical Label* | *Z-max* | *x* | *y* | *z* |
|---|---|---|---|---|
| *Positive Behavioral Modulation (Increased Activation for Greater Distance from the Arc)* | | | | |
| Supplementary motor cortex, SMA | 6.67 | 0 | 4 | 50 |
| Right superior parietal lobule, 7A | 5.08 | 8 | −54 | 64 |
| Right inferior parietal lobule, PGp | 5.28 | 40 | −80 | 20 |
| Left sensorimotor cortices, PMd/M1/S1 | 6.21 | −38 | −22 | 58 |
| Right frontal operculum | 5.02 | 44 | 16 | 2 |
| Right cerebellum lobule V/VI | 5.99 | 18 | −52 | −20 |
| Left visual cortex V5/MT | 5.83 | −48 | −66 | 4 |
| Right inferior parietal lobule, PFt | 5.29 | 60 | −22 | 40 |
| Right cerebellum lobule VIII | 5.35 | 12 | −60 | −50 |
| Left visual cortex V4 | 5.24 | −20 | −88 | −10 |
| Right dorsal premotor cortex, PMd | 5.33 | 22 | −2 | 72 |
| Right visual cortex V1/V2 | 5.28 | 14 | −88 | −4 |
| Right primary somatosensory cortex, S1 | 5.14 | 42 | −42 | 64 |
| Left cerebellum crus I | 4.31 | −42 | −52 | −28 |
| Right middle frontal gyrus | 4.73 | 26 | 6 | 50 |
| Left cerebellum lobule VI | 4.45 | −30 | −52 | −28 |
| *Negative Behavioral Modulation (Increased Activation for Lower Distance from the Arc)* | | | | |
| Right putamen | 5.22 | 20 | 12 | −8 |
| Left putamen | 5.03 | −18 | 14 | −8 |
| Left orbitofrontal cortex | 4.77 | −32 | 58 | −4 |

The coordinates are according to the MNI standard template. *Z* values indicate the local maxima obtained from the group positive or negative behavioral modulation maps.

(Figure 5B, second row). In both these cases, RS-FC was found to be not significantly different from zero at baseline and to become positive following training, and this is to a greater extent for participants who improved their motor performance more. It can also be seen that a seed in lobule VIII of the cerebellum revealed a learning-related increase in RS-FC with area V5/MT on the right side (Figure 5C, third row). The RS-FC between these two areas was positive already at baseline and became significantly more positive as a result of motor learning. A learning-related change in RS-FC was also observed between the seed in the left ventral putamen and a cluster in the left middle temporal gyrus (MTG; Figure 5D, fourth row). The functional connectivity between these two areas was negative at baseline ($p = .032$) and was no longer significantly different from zero following training ($t$ test relative to zero at posttraining: $p = .104$), suggesting that following training the two areas became functionally decoupled. When seeds were placed in left M1 and OFC, we observed changes in RS-FC that were not significantly correlated with the change in motor performance at the significance threshold adjusted for multiple comparisons, and therefore, these findings were not taken as correlates of motor learning (seed–target cluster [MNI coordinates of the peak]: left M1–right SII [68, −24, 14]: $r = -.26$, $p = .27$; OFC–right thalamus [8, −16, 12]: $r = .43$, $p = .057$).

For each cluster that showed learning-related changes in RS-FC, we asked whether the changes in resting brain connectivity were related to the positive or negative behavioral modulation maps. For this purpose, we ran conjunction analyses between the clusters identified in the RS-FC analyses and the portions of the positive and negative behavioral modulation map involved in performing the task (i.e., Figures 3 and 4, first and second row). Figure 5 only shows the findings related to the intersection between the RS-FC analyses and the movement map (the intersection between the RS-FC analyses and the intermovement map was empty for the most part; when an overlap was found, it was similar in location to

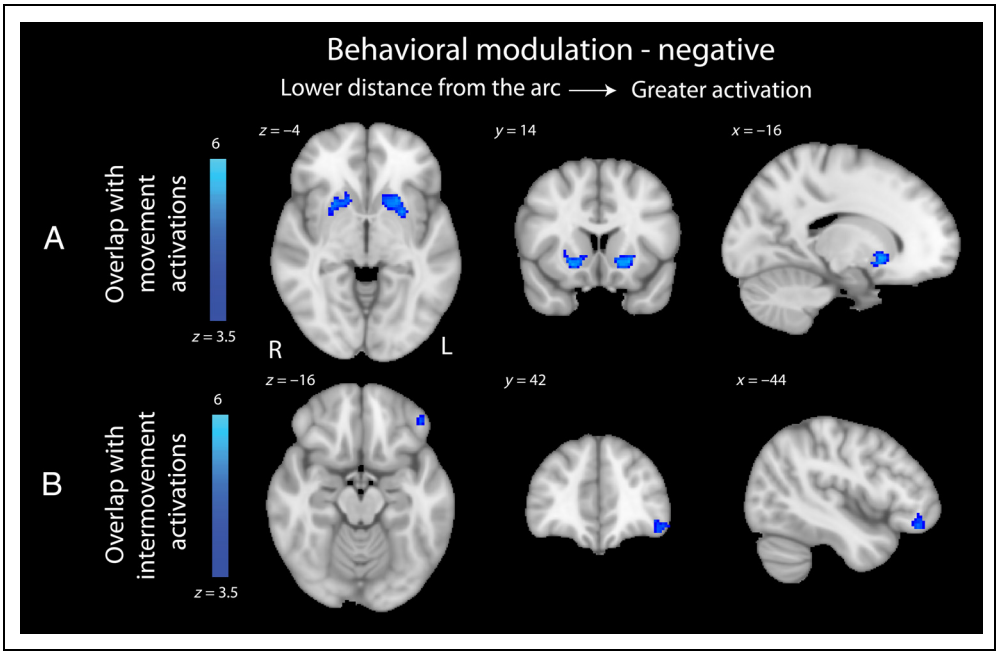


**Figure 4.** Task-based activations related to movement accuracy. Shown are the areas of the brain that were significantly more activated in trials with lower distance from the arc, that is, showing a negative behavior-dependent modulation of the neural responses. The first row shows the results of the conjunction analysis between the negative behavioral modulation map on the one hand and the areas showing increased activations during movement execution (movement regressor) on the other hand. The second row shows the results of the conjunction analysis between the negative behavioral modulation map and the areas showing increased activations during the intermovement epochs (intermovement regressor). Areas showing increased activations for lower distance from the arc included the ventral putamen, the nucleus accumbens, and the left OFC. R = right hemisphere; L = left hemisphere. The *x*, *y*, and *z* coordinates of cross-sections are reported in MNI space.

the movement map, but more limited in extent, and is not shown). It can be seen that most changes in RS-FC were contained within the positive behavioral modulation map (i.e., areas showing greater activation for greater distance from the arc). The clusters showing learning-related changes in RS-FC, namely, lobule VI of the cerebellum (Figure 5, first row), primary and premotor areas (second row), and visual area V5/MT (third row), as well as the seeds in PMd, CB-VI, and CB-VIII, all largely overlapped the areas that were shown to increase activation when movement error was higher. The RS-FC change maps and the positive behavioral modulation maps were highly consistent in terms of their location in the brain. This can be seen in Figure 5 from the nearly complete overlap (yellow overlay) between the RS-FC clusters (green maps) and the error-related clusters from the task-based part of the study (red maps).

The seed in the ventral putamen overlapped, by design, the negative behavioral modulation map (i.e., areas showing greater activation for greater accuracy). However, the cluster in the left MTG that showed decreased connectivity with the putamen seed was outside the movement or intermovement task-positive map (areas significantly more active during task execution compared with rest), as well as outside the areas showing positive or negative behavioral modulation. No other areas showing greater activation for movement of greater accuracy were found to overlap the RS-FC maps.

### Post hoc Analysis of Additional Seeds

The task-based behavioral modulation analyses shown in Table 2 revealed areas of potential interest that were not part of the initial RS-FC analysis plan, particularly the SMA, the inferior and superior parietal lobules and the ventral putamen in the right hemisphere. To clarify whether important changes in RS-FC may be found in relation to these areas, we ran additional RS-FC analyses, placing four additional seeds at the location of peak activation for these areas. The coordinates for the seeds were derived from the peaks of the behavioral modulation maps, rather than from the task-based activation maps (MNI coordinates: SMA: 0, 4, 50; superior parietal lobule: 8, −54, 64; inferior parietal lobule: 40, −80, 20; right putamen: 20, 12, −8). Owing to their exploratory nature, these analyses were conducted at the less conservative threshold of $p = .01$. This threshold was utilized to assess cluster significance, to assess the significance of the correlation between change in functional connectivity and motor learning, as well as to assess the significance of the change from pre- to posttraining in functional connectivity scores. These analyses did not reveal areas in the brain where the change in RS-FC was reliably correlated with improvement in motor performance.

### The Role of Movement Timing Accuracy

Several areas whose activity during task was modulated by spatial error were identified. In principle, it is possible that the effect of spatial error in these areas was influenced by duration-based feedback, because these two measures are correlated behaviorally. To address this potential confound, we ran a variant of the previously described analysis of the task data, where we split each

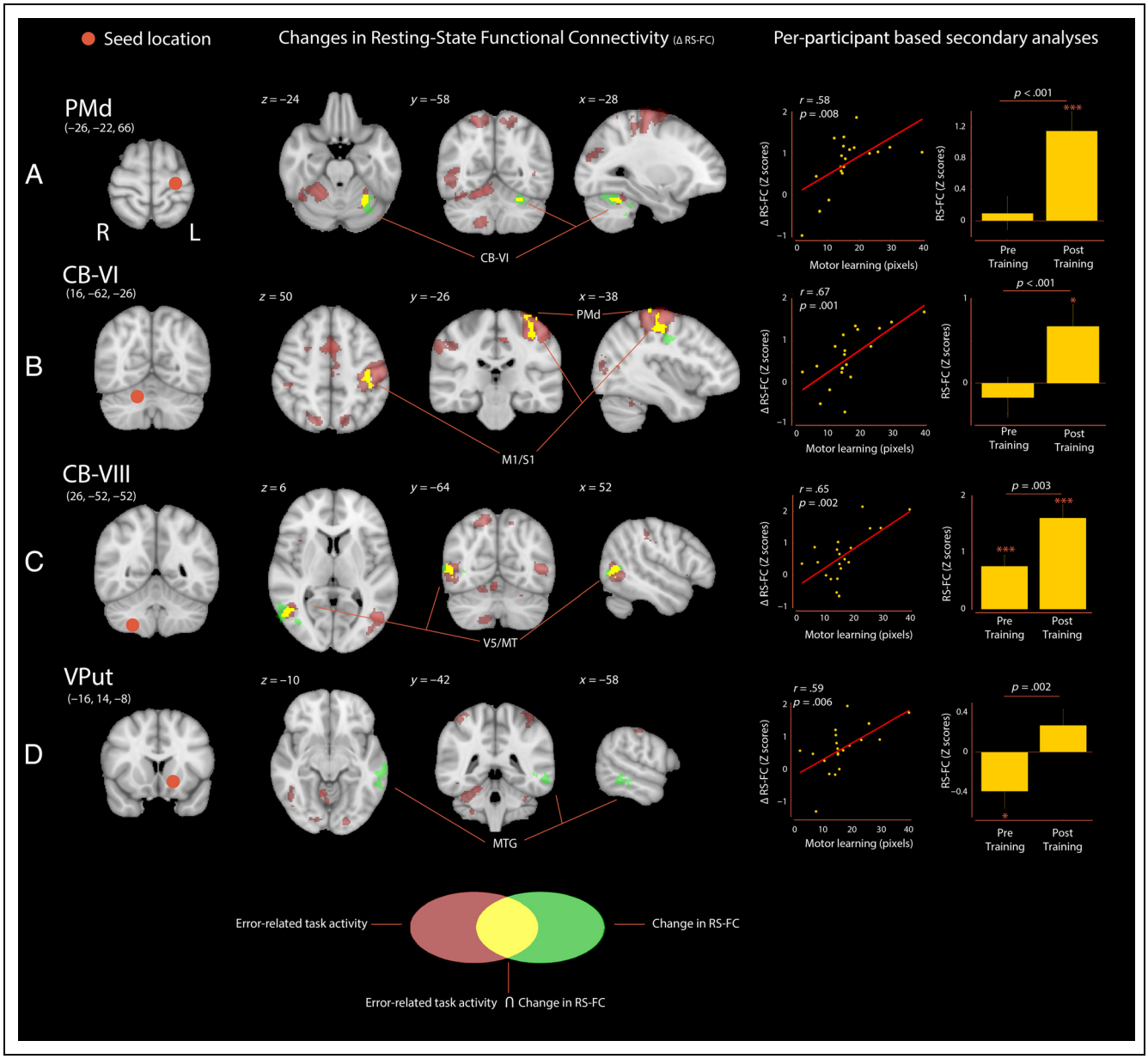


**Figure 5.** Changes in RS-FC related to motor learning. The first column shows the location of the seeds for the RS-FC analyses. The three central columns show the areas of the brain that increased their RS-FC with each seed in a learning-dependent fashion, that is, exhibiting greater change in RS-FC for participants who improved their motor performance more. The green maps show the entirety of the map showing learning-related changes in RS-FC. The red maps show the areas of the brain where greater activations were observed for increased distance from the arc during the task, that is, areas showing positive behavioral modulation (themselves the results of a conjunction analysis with the movement-related activations; see Figure 3). The yellow overlay shows the results of the conjunction analysis between the RS-FC maps and the task-based positive behavioral modulation maps. Changes in the resting-state maps were mostly found in areas that overlapped the positive behavioral modulation, particularly the cerebellum, the dorsal premotor cortex, the primary motor and sensory cortices, and area V5/MT. No regions in the RS-FC analyses, other than the seed in ventral putamen, were found to overlap areas of the brain with negative behavioral modulation. The two columns on the right-hand side of each row give mean measures of connectivity before and after motor training and the correlation coefficient between the change in RS-FC and changes in motor performance. R = right hemisphere; L = left hemisphere; PMd = dorsal premotor cortex; CB = cerebellum; VPut = ventral putamen; M1 = primary motor cortex; S1 = primary somatosensory cortex; V5/MT = middle temporal visual area. The *x*, *y*, and *z* coordinates of cross-sections are reported in MNI space.

of the explanatory variables shown in Figure 1D and E in two: one corresponding to the trials with accurate timing (movement duration within the prescribed window, yielding green feedback signal, henceforth referred to as "successful trials"; 62% of the trials) and the other corresponding to the remaining trials (38%).

We found that trials performed within the correct time window were associated with stronger activations of bilateral putamen, including the nucleus accumbens, bilateral higher-order visual cortices, bilateral superior parietal lobule (7A), bilateral dorsal premotor cortex, and cerebellar vermis VIII. Conversely, trials

**Table 3.** Conjunction of RS-FC Maps and Behavioral Modulation Maps

| *Seed* | *Target* | *Z-max* | *x* | *y* | *z* |
|---|---|---|---|---|---|
| *Overlap with Positive Behavioral Modulation—Movement Map* | | | | | |
| Left PMd | Left cerebellum lobule VI | 4.0 | −28 | −58 | −24 |
| Right CB-VI | Left primary somatosensory cortex | 3.5 | −38 | −24 | 50 |
| Right CB-VI | Left primary motor cortex | 2.6 | −36 | −28 | 60 |
| Right CB-VI | Left dorsal premotor cortex | 2.4 | −32 | −26 | 70 |
| Right CB-VIII | Right visual cortex V5/MT | 3.8 | 48 | −68 | 0 |
| *Overlap with Positive Behavioral Modulation—Intermovement Map* | | | | | |
| Left PMd | Left cerebellum lobule VI | 2.9 | −26 | −62 | −26 |
| Right CB-VIII | Right visual cortex V5/MT | 2.8 | 46 | −56 | −8 |

The coordinates are according to the MNI standard template. *Z*-max values indicate the local maxima obtained from the group map of the learning-related changes in RS-FC.

with incorrect movement duration showed stronger activation of right inferior parietal lobule, bilateral temporo-occipital junction, bilateral primary and secondary somatosensory cortex, bilateral insula, posterior cingulate cortex, and left parahippocampal gyrus.

More importantly for the question investigated here, we also ran a contrast between the behavioral modulation maps for spatial error generated by trials that were successful versus unsuccessful in terms of movement duration. If the behavioral modulation maps shown in Figures 3 and 4 primarily reflected brain activity proportional to spatial error, then their patterns should be virtually identical regardless of whether such maps were generated from trials with successful or unsuccessful movement duration. Conversely, if success in the duration dimension plays a significant role in the pattern of spatial behavioral modulation, the behavioral modulation maps should differ depending on whether they are computed from successful versus unsuccessful trials. We found that the contrast between the spatial behavioral modulation maps for the successful versus unsuccessful trials (duration-based) was mostly empty This suggests that the association that we previously observed between brain activity and spatial error during learning is not driven by differences in temporal accuracy and any potential rewarding effect associated with it.

Although the task-based behavioral modulation maps appear to primarily reflect the amount of spatial error, rather than timing accuracy, it is still possible that the changes in RS-FC observed after learning may be related to the improvement in timing accuracy. Our approach to investigate this possibility was identical to the RS-FC analyses we previously ran, except for the behavioral factor, which here was the change in duration-based success rate, rather than the change in spatial error. The findings of this resting-state analysis are shown in Table 4. The conjunction analyses between the RS-FC and task-based timing-related maps revealed no area of significant overlap.

In summary, the timing analyses revealed that (1) different networks were activated for movements with successful versus unsuccessful duration, (2) the modulation of brain responses by the amount of spatial error was not confounded by the success of movement in the timing domain, and (3) the learning-related changes in the timing domain found in the resting brain did not overlap areas of the brain that during task showed responses related to timing accuracy.

**Table 4.** RS-FC Maps Related to Improvements in Movement Timing

| *Seed* | *Target* | *Z-max* | *x* | *y* | *z* | *Voxels* | *FC Pre* | *FC Post* | *FC Change (p)* |
|---|---|---|---|---|---|---|---|---|---|
| Right CB-VIII | Left V5/MT | 3.7 | −38 | −82 | 6 | 375 | 0.51 | 1.26 | .002 |
| Left ventral putamen | Right SII | 4.25 | 52 | −26 | 20 | 479 | 1.7 | 0.83 | .006 |

The coordinates are according to the MNI standard template. Functional connectivity (FC) at pre- and posttraining are expressed as *Z* scores, in relation to the entire cluster revealed by the RS-FC analysis.

## DISCUSSION

We identified two widespread brain networks in which activations during a motor learning task were correlated, positively or negatively, with movement error. We then asked which of these activations are maintained in the form of changes in RS-FC observable following training. We found that the majority of the connectivity changes in the resting brain following motor learning occurred in areas where activation during the task scaled with the quality of motor performance. Furthermore, it was found that most of the changes in connectivity at rest overlap areas of the brain that show increased activation with increased movement error during the task and do not overlap areas that show increased activation with decreased movement error. This suggests that task-based activations propagate into subsequent resting-state activity predominantly in the form of a movement error network, centered on areas within the cerebellum, with additional contributions from visual, somatosensory, and cortical motor areas. The activity of this network changed from prelearning to postlearning scans in proportion to the amount of motor learning, suggesting that these changes are associated with the initial stages of motor memory formation.

### Error-related Task Activations

Several areas of the cerebellum were found to increase their activation in proportion to the distance from the arc. These included lobules VI, VIII, and Crus I, all bilaterally, lobule V on the right side, and an area of the medial cerebellum, extending from lobules VI and VIII of the vermis to the spinocerebellar component of lobules VI and VIII, most prominently in the right cerebellar hemisphere. This finding is compatible with the involvement of the cerebellum in the processing of movement errors, as evidenced by a large body of previous work (see Hardwick, Rottschy, Miall, & Eickhoff, 2013, for a review). Patients suffering from cerebellar lesions have been found to have impaired ability to compensate for both dynamic and kinematic errors (Izawa, Criscimagna-Hemminger, & Shadmehr, 2012; Criscimagna-Hemminger et al., 2010). Cerebellar activity has been consistently detected in previous neuroimaging studies of motor learning (Shmuelof et al., 2014; Debas et al., 2010; Seidler, Noll, & Chintalapati, 2006) and has been specifically linked on a trial-by-trial basis to movement error (Schlerf, Ivry, & Diedrichsen, 2012; Diedrichsen et al., 2005). The involvement of lobules V–VI–VIII is consistent with the somatotopic organization of cerebellar maps for the control of the wrist, hand, and fingers (Manni & Petrosini, 2004). The additional involvement of the cerebellar vermis may reflect adjustments to an eye–hand coordinated predictive system (Voogd, Schraa-Tam, van der Geest, & De Zeeuw, 2012). One possibility is that, as a result of training, gaze shifts would be timed to provide high-resolution visual information of cursor position that is needed to accurately perform the submovements involved in this task (Bowman, Johannson, & Flanagan, 2009; Johansson, Westling, Bäckström, & Flanagan, 2001).

Other areas that showed increased activation during the task in proportion to the distance from the arc include the visual cortex; the superior and inferior parietal lobules; and primary somatosensory, motor, and premotor cortices. These activations are again compatible with an error-processing mechanism, based on recent observations in monkeys that both primary motor and premotor cortices encode information on end-point errors in reaching (Inoue, Uchimura, & Kitazawa, 2016). Activations in M1 have also been found to correlate with the speed and accuracy of sequential finger movements (Karni et al., 1995), suggesting a role in the acquisition and generation of skilled movements. The posterior parietal cortex is believed to play a role in the calibration of visually guided movements (Clower et al., 1996), for example, in establishing and updating a mapping between visual and proprioceptive representations of hand position. The responses in primary somatosensory cortex may likewise involve sensory error processing during learning. This possibility is supported by recent evidence in mice in which optogenetic photoinhibition of primary somatosensory cortex impaired the acquisition of a novel motor adaptation, but not the execution of already adapted movements (Mathis, Mathis, & Uchida, 2017).

Several other areas were found to show greater activity in trials with low distance from the arc, that is, for movements with greater movement accuracy. Clusters with this form of response were found in the ventral putamen and nucleus accumbens bilaterally and in the left OFC. These areas have been shown to play a role in mediating the rewarding value of conditioned and unconditioned stimuli (Levita et al., 2009; Daw, O'Doherty, Dayan, Seymour, & Dolan, 2006; O'Doherty et al., 2003; Ramnani & Miall, 2003). Although there is no explicit manipulation of reward for spatial accuracy in this study, the activations observed in this reward network are presumably related to the implicit reward associated with successful movement. The reinforcement of successful action is increasingly understood as an important mechanism in motor learning. This form of learning may be based on dopamine-dependent selection of successful patterns of neural activity based on the conjunction of sensory afferent activity, motor output activity, and temporally related firing of dopamine cells (Wickens et al., 2003). Reward-based motor learning would complement adjustments to feedforward control made possible by error-based mechanisms, with the relative importance of these two mechanisms being determined by the nature of the task and the availability of reward versus error signals (Haith & Krakauer, 2013; Izawa & Shadmehr, 2011). Importantly, the purpose of the current study

was not to dissociate the brain mechanisms for error-based and reward-based forms of motor learning. In fact, there was no independent manipulation of error and rewards in our experiment, and an explicit reinforcement signal was only provided for the timing dimension. The partial or complete absence of explicit reinforcements is a common feature in motor learning outside the laboratory, which motivated our design choice. Nevertheless, there is a considerable overlap between (a) the areas we found to be more active for lower spatial error, (b) the areas we found to be more active in presence of positive duration-based binary feedback, and (c) the reward-based network reported previously. This suggests that reward may play a role during the task-related activity even when limited explicit/external reward signal is provided to participants.

### From Error-related Task Activations to Learning-related Changes in RS-FC

The most prominent effect of motor learning on the resting brain connectivity was a strengthening in proportion to learning of the connectivity between lobule VI of the cerebellum and a cluster comprising primary motor, dorsal premotor, and primary somatosensory cortex. These changes in functional connectivity are presumably based on the anatomical connections through the thalamus between the cerebellum and primary motor (Dum & Strick, 2003), somatosensory (Schmahmann & Pandya, 1992; Glickstein, May, & Mercier, 1985), and dorsal premotor cortex (Hashimoto et al., 2010). The strengthening of connections between the cerebellum and premotor as well as primary motor and sensory areas as a result of motor learning has been documented previously for both motor adaptation (Vahdat et al., 2011) and motor skill learning (Philip & Frey, 2016). However, these and other previous studies used either resting-state or task-based imaging in isolation, which reduces the possibility to directly link the changes observed at rest following training with the neural activations observed during the task. Conversely, this study integrated both imaging techniques as part of a coherent design with the explicit goal to explore links between these two types of brain activity.

Learning-related changes in RS-FC were also detected between the cerebellum and the middle temporal visual area (V5/MT). This area is known to play a role in the perception of motion (Tootell et al., 1995; Zeki, 1974). Area MT/V5 has reciprocal connections to the cerebellum by corticopontine projections through the dorsolateral pontine nuclei (Xiong & Nagao, 2002; Glickstein et al., 1994; Maunsell & Van Essen, 1983). The density of the connections between the cerebellum and visual areas has suggested that the cerebellum may provide a primary link between visual and motor areas (Glickstein, 2007). The increase in functional connectivity between visual and cerebellar areas observed in this study may reflect an increased ability to process the movement of the cursor on the screen and to generate coordinated eye–hand responses.

A primary aim of this study was to determine whether changes in RS-FC associated with motor learning are mainly an expression of the areas that increase their activation during trials with greater movement error or areas that increase their activation during trials with greater movement accuracy. The results of conjunction analyses, which assess the overlap between task-related activity and resting-state networks, indicate that most of the changes that persist following learning involved brain areas with the former type of responses, in particular lobules VI and VIII of cerebellar cortex, dorsal premotor cortex, primary motor and somatosensory cortices, and area V5/MT. Notably, the cerebellum appeared in each of these functional connectivity findings, either as the origin seed location or as the target area. This observation is compatible with the idea that the cerebellum is central to the formation of early motor memories, and as this study shows, its participation is not restricted to adaptation involving prior learning (Shadmehr, 2010).

The current findings reveal that the error-processing network is extensive and includes not only cerebellum but also visual and somatosensory cortices and areas assumed to plan and perform movements, such as the parietal, premotor, and motor cortices. The current findings also suggest that motor memories could emerge in the form of increased connectivity between the areas responsible for sensory error processing during learning. This is shown here in the form of learning-related changes in the spontaneous activity of the brain immediately following task execution. This observation will have to be complemented by recordings of brain activity at longer time intervals, as it has been reported that the networks for short and long-term retention may differ. For example, a recent study (Della-Maggiore, Villalta, Kovacevic, & McIntosh, 2017) has shown that the increase in RS-FC within a network comprising motor, premotor, posterior parietal cortex, cerebellum, and putamen correlated positively with long-term retention of a motor adaptation but negatively with short-term retention. This observation suggests that short-term and long-term memory formation may be based on partly different neural processes, at least in the case of motor adaptation. In the current experiment, the resting-state scans immediately following task completion would correspond to short-term retention of motor memories in the Della-Maggiore et al. (2017) study. It would be useful in future studies of motor skill learning to record from the resting brain at longer time intervals to gauge long-term retention. On the other hand, the current study differs from Della-Maggiore et al. (2017) in that we specifically investigated the relationship between task-based activations and subsequent patterns of RS-FC, whereas this previous study was entirely based on changes in RS-FC at different timescales.

The contribution of the areas responsive to high movement accuracy was limited in the current study, compared

with the extensive involvement of the error-related network, as well as compared with previous studies on reinforcement-based motor learning (Sidarta et al., 2016). The present analyses revealed a change in RS-FC involving a seed in the ventral putamen, an area that was activated in proportion to movement accuracy and that has been implicated in the processing of rewarding stimuli (O'Doherty et al., 2003). The functional significance of this finding is unclear. The target cluster of the putamen seed is in the MTG, an area outside the positive or negative behavioral modulation maps, and for which a function in relation to motor control is not unequivocally established (but see Della-Maggiore & McIntosh, 2005, for a previous motor learning study reporting a cluster in a similar location). Furthermore, the pattern of change in RS-FC shows that the connectivity between putamen and MTG decreases and approaches zero in association with motor learning. We can speculate that the connectivity in the brain related to movement success may be more important early in learning and that this role becomes less prominent as training progresses and overall performance improves. Alternatively, the decrease in connectivity may reflect an increase capacity of the brain to perform certain computations. In some cases, correlations in neural signals have been shown to limit the amount of information available to the system (Moreno-Bote et al., 2014). Although at present difficult to interpret, this finding is potentially interesting as it shows a pattern distinct from the rest of our findings, in that (1) the magnitude of RS-FC decreases rather than increasing and (2) the target cluster in MTG is not part of the network activated when performing the task. The specific nature of the task employed here may have also contributed to the limited role of the areas responsive to movement accuracy. A recent behavioral study has shown that, when reliable sensory feedback is available, motor learning is driven almost exclusively by movement error (Izawa & Shadmehr, 2011). These authors also showed that reward becomes more important for learning in the presence of degraded sensory feedback. The presence of high-quality sensory feedback in our study could help explain the predominance of error-based traces in our resting-state data. Future studies could directly contrast error-based and reward-based motor learning, for example, by modulating the reliability of sensory feedback, and investigate the persisting changes they elicit in the pattern of RS-FC.

In principle, it could be argued that changes in RS-FC could reflect simply how much a given network has been recruited in the recent past, as in a use-dependent form of plasticity (Diedrichsen, White, Newman, & Lally, 2010), rather than to the formation of novel motor memories. This is unlikely to explain the pattern of findings presented here, because the changes in RS-FC were correlated with the amount of motor learning on a per-participant basis. Furthermore, if the changes in RS-FC were solely a by product of use-dependent plasticity, one would expect functional connectivity to closely resemble the task-based activations, including the areas activated by trials in which motor accuracy is high. This should particularly be the case given that motor performance is better toward the end of the training. Contrary to this prediction, only part of the networks implicated in the task is found in the subsequent resting state. In particular, it is found that the changes in RS-FC primarily reflect the areas that become active in presence of high-error trials, despite the fact that such events are prominent earlier in training.

In conclusion, our findings suggest that, during the active stages of motor learning, the brain utilizes feedback related to both error and accuracy to improve movements on a trial-by-trial basis. Activations attributable to error processing are widespread and involve areas in cerebellum as well as frontal and parietal cortices. Persistent learning-related changes in connectivity reflect this error-related task-based activation. The final product of motor learning is reflected off-line primarily in increases in connectivity between the cerebellum and the premotor and primary sensorimotor cortices, carrying the signature of an error-driven process.


## Acknowledgments

This study was supported by the National Institute of Child Health and Human Development (NICHD R01 HD075740) and by Fonds de recherche du Québec–Nature et technologies.



Reprint requests should be sent to David J. Ostry, Department of Psychology, McGill University, 2001 McGill College, H3A 1G1, Montreal, Quebec, Canada, or via e-mail: david.ostry@mcgill.ca.


## REFERENCES


Albert, N. B., Robertson, E. M., & Miall, R. C. (2009). The resting human brain and motor learning. *Current Biology*, *19*, 1023–1027.

Bowman, M. C., Johannson, R. S., & Flanagan, J. R. (2009). Eye–hand coordination in a sequential target contact task. *Experimental Brain Research*, *195*, 273–283.

Brashers-Krug, T., Shadmehr, R., & Bizzi, E. (1996). Consolidation in human motor memory. *Nature*, *382*, 252–255.

Clower, D. M., Hoffman, J. M., Votaw, J. R., Faber, T. L., Woods, R. P., & Alexander, G. E. (1996). Role of posterior parietal cortex in the recalibration of visually guided reaching. *Nature*, *383*, 618–621.

Criscimagna-Hemminger, S. E., Bastian, A. J., & Shadmehr, R. (2010). Size of error affects cerebellar contributions to motor learning. *Journal of Neurophysiology*, *103*, 2275–2284.

Daw, N. D., O'Doherty, J. P., Dayan, P., Seymour, B., & Dolan, R. J. (2006). Cortical substrates for exploratory decisions in humans. *Nature*, *441*, 876–879.

Debas, K., Carrier, J., Orban, P., Barakat, M., Lungu, O., Vandewalle, G., et al. (2010). Brain plasticity related to the consolidation of motor sequence learning and motor adaptation. *Proceedings of the National Academy of Sciences, U.S.A.*, *107*, 17839–17844.

Della-Maggiore, V., & McIntosh, A. R. (2005). Time course of changes in brain activity and functional connectivity associated with long-term adaptation to a rotational transformation. *Journal of Neurophysiology*, *93*, 2254–2262.

Della-Maggiore, V., Villalta, J. I., Kovacevic, N., & McIntosh, A. R. (2017). Functional evidence for memory stabilization in sensorimotor adaptation: A 24-h resting-state fMRI study. *Cerebral Cortex*, *27*, 1748–1757.

Diedrichsen, J., Balsters, J. H., Flavell, J., Cussans, E., & Ramnani, N. (2009). A probabilistic MR atlas of the human cerebellum. *Neuroimage*, *46*, 39–46.

Diedrichsen, J., Hashambhoy, Y., Rane, T., & Shadmehr, R. (2005). Neural correlates of reach errors. *Journal of Neuroscience*, *25*, 9919–9931.

Diedrichsen, J., White, O., Newman, D., & Lally, N. (2010). Use-dependent and error-based learning of motor behaviors. *Journal of Neuroscience*, *30*, 5159–5166.

Doyon, J., Song, A. W., Karni, A., Lalonde, F., Adams, M. M., & Ungerleider, L. G. (2002). Experience-dependent changes in cerebellar contributions to motor sequence learning. *Proceedings of the National Academy of Sciences, U.S.A.*, *99*, 1017–1022.

Dum, R. P., & Strick, P. L. (2003). An unfolded map of the cerebellar dentate nucleus and its projections to the cerebral cortex. *Journal of Neurophysiology*, *89*, 634–639.

Eickhoff, S. B., Stephan, K. E., Mohlberg, H., Grefkes, C., Fink, G. R., Amunts, K., et al. (2005). A new SPM toolbox for combining probabilistic cytoarchitectonic maps and functional imaging data. *Neuroimage*, *25*, 1325–1335.

Fitts, P. M. (1954). The information capacity of the human motor system in controlling the amplitude of movement. *Journal of Experimental Psychology*, *47*, 381–391.

Friston, K., Ashburner, J., Frith, C. D., Poline, J. B., Heather, J. D., & Frackowiak, R. S. J. (1995). Spatial registration and normalization of images. *Human Brain Mapping*, *3*, 165–189.

Glickstein, M. (2007). What does the cerebellum really do? *Current Biology*, *17*, R824–R827.

Glickstein, M., Gerrits, N., Kralj-Hans, I., Mercier, B., Stein, J., & Voogd, J. (1994). Visual pontocerebellar projections in the macaque. *Journal of Comparative Neurology*, *349*, 51–72.

Glickstein, M., May, J. G., & Mercier, B. E. (1985). Corticopontine projection in the macaque: The distribution of labelled cortical cells after large injections of horseradish peroxidase in the pontine nuclei. *Journal of Comparative Neurology*, *235*, 343–359.

Gregory, M. D., Agam, Y., Selvadurai, C., Nagy, A., Vangel, M., Tucker, M., et al. (2014). Resting state connectivity immediately following learning correlates with subsequent sleep-dependent enhancement of motor task performance. *Neuroimage*, *102*, 666–673.

Greve, D. N., & Fischl, B. (2009). Accurate and robust brain image alignment using boundary-based registration. *Neuroimage*, *48*, 63–72.

Griffanti, L., Douaud, G., Bijsterbosch, J., Evangelisti, S., Alfaro-Almagro, F., Glasser, M. F., et al. (2017). Hand classification of fMRI ICA noise components. *Neuroimage*, *154*, 188–205.

Haith, A. M., & Krakauer, J. W. (2013). Model-based and model-free mechanisms of human motor learning. In M. Richardson, M. Riley, & K. Shockley (Eds.), *Progress in motor control* (1st ed., pp. 1–21). New York: Springer.

Hardwick, R. M., Rottschy, C., Miall, R. C., & Eickhoff, S. B. (2013). A quantitative meta-analysis and review of motor learning in the human brain. *Neuroimage*, *67*, 283–297.

Hashimoto, M., Takahara, D., Hirata, Y., Inoue, K. I., Miyachi, S., Nambu, A., et al. (2010). Motor and non-motor projections from the cerebellum to rostrocaudally distinct sectors of the dorsal premotor cortex in macaques. *European Journal of Neuroscience*, *31*, 1402–1413.

Howard, J. D., Gottfried, J. A., Tobler, P. N., & Kahnt, T. (2015). Identity-specific coding of future rewards in the human orbitofrontal cortex. *Proceedings of the National Academy of Sciences, U.S.A.*, *112*, 5195–5200.

Huang, V. S., Haith, A., Mazzoni, P., & Krakauer, J. W. (2011). Rethinking motor learning and savings in adaptation paradigms: Model-free memory for successful actions combines with internal models. *Neuron*, *70*, 787–801.

Inoue, M., Uchimura, M., & Kitazawa, S. (2016). Error signals in motor cortices drive adaptation in reaching. *Neuron*, *90*, 1114–1126.

Izawa, J., Criscimagna-Hemminger, S. E., & Shadmehr, R. (2012). Cerebellar contributions to reach adaptation and learning sensory consequences of action. *Journal of Neuroscience*, *32*, 4230–4239.

Izawa, J., & Shadmehr, R. (2011). Learning from sensory and reward prediction errors during motor adaptation. *PLoS Computational Biology*, *7*, e1002012.

Johansson, R. S., Westling, G., Bäckström, A., & Flanagan, J. R. (2001). Eye–hand coordination in object manipulation. *Journal of Neuroscience*, *21*, 6917–6932.

Karni, A., Meyer, G., Jezzard, P., Adams, M. M., Turner, R., & Ungerleider, L. G. (1995). Functional MRI evidence for adult motor cortex plasticity during motor skill learning. *Nature*, *377*, 155–158.

Kelly, R. E., Alexopoulos, G. S., Wang, Z., Gunning, F. M., Murphy, C. F., Morimoto, S. S., et al. (2010). Visual inspection of independent components: Defining a procedure for artifact removal from fMRI data. *Journal of Neuroscience Methods*, *189*, 233–245.

Levita, L., Hare, T. A., Voss, H. U., Glover, G., Ballon, D. J., & Casey, B. J. (2009). The bivalent side of the nucleus accumbens. *Neuroimage*, *44*, 1178–1187.

Lewis, C. M., Baldassarre, A., Committeri, G., Romani, G. L., & Corbetta, M. (2009). Learning sculpts the spontaneous activity of the resting human brain. *Proceedings of the National Academy of Sciences, U.S.A.*, *106*, 17558–17563.

Lutz, K., Pedroni, A., Nadig, K., Luechinger, R., & Jäncke, L. (2012). The rewarding value of good motor performance in the context of monetary incentives. *Neuropsychologia*, *50*, 1739–1747.

Manni, E., & Petrosini, L. (2004). A century of cerebellar somatotopy: A debated representation. *Nature Reviews Neuroscience*, *5*, 241–249.

Mathis, M. W., Mathis, A., & Uchida, N. (2017). Somatosensory cortex plays an essential role in forelimb motor adaptation in mice. *Neuron*, *93*, 1493–1503.

Maunsell, J. H. R., & van Essen, D. C. (1983). The connections of the middle temporal visual area (MT) and their relationship to a cortical hierarchy in the macaque monkey. *Journal of Neuroscience*, *3*, 2563–2586.

Miall, R. C., & Wolpert, D. M. (1996). Forward models for physiological motor control. *Neural Networks*, *9*, 1265–1279.

Moeller, S., Yacoub, E., Olman, C. A., Auerbach, E., Strupp, J., Harel, N., et al. (2010). Multiband multislice GE-EPI at 7 tesla, with 16-fold acceleration using partial parallel imaging with application to high spatial and temporal whole-brain fMRI. *Magnetic Resonance in Medicine*, *63*, 1144–1153.

Moreno-Bote, R., Beck, J., Kanitscheider, I., Pitkow, X., Latham, P., & Pouget, A. (2014). Information-limiting correlations. *Nature Neuroscience*, *17*, 1410–1417.

O'Doherty, J. P., Dayan, P., Friston, K., Critchley, H., & Dolan, R. J. (2003). Temporal difference models and reward-related learning in the human brain. *Neuron*, *38*, 329–337.

Philip, B. A., & Frey, S. H. (2016). Increased functional connectivity between cortical hand areas and praxis network associated with training-related improvements in non-dominant hand precision drawing. *Neuropsychologia*, *87*, 157–168.

Pruim, R. H., Mennes, M., van Rooij, D., Llera, A., Buitelaar, J. K., & Beckmann, C. F. (2015). ICA-AROMA: A robust ICA-based

strategy for removing motion artifacts from fMRI data. *Neuroimage*, *112*, 267–277.
Ramnani, N., & Miall, R. C. (2003). Instructed delay activity in the human prefrontal cortex is modulated by monetary reward expectation. *Cerebral Cortex*, *13*, 318–327.
Schlerf, J., Ivry, R. B., & Diedrichsen, J. (2012). Encoding of sensory prediction errors in the human cerebellum. *Journal of Neuroscience*, *32*, 4913–4922.
Schmahmann, J. D., & Pandya, D. N. (1992). Course of the fiber pathways to pons from parasensory association areas in the rhesus monkey. *Journal of Comparative Neurology*, *326*, 159–179.
Schultz, W. (1998). Predictive reward signal of dopamine neurons. *Journal of Neurophysiology*, *80*, 1–27.
Seidler, R. D., Noll, D. C., & Chintalapati, P. (2006). Bilateral basal ganglia activation associated with sensorimotor adaptation. *Experimental Brain Research*, *175*, 544–555.
Setsompop, K., Gagoski, B. A., Polimeni, J. R., Witzel, T., Wedeen, V. J., & Wald, L. L. (2012). Blipped-controlled aliasing in parallel imaging for simultaneous multislice echo planar imaging with reduced g-factor penalty. *Magnetic Resonance in Medicine*, *67*, 1210–1224.
Shadmehr, R. (2010). Control of movements and temporal discounting of reward. *Current Opinion in Neurobiology*, *20*, 726–730.
Shehzad, Z., Kelly, A. C., Reiss, P. T., Gee, D. G., Gotimer, K., Uddin, L. Q., et al. (2009). The resting brain: Unconstrained yet reliable. *Cerebral Cortex*, *19*, 2209–2229.
Shmuelof, L., Krakauer, J. W., & Mazzoni, P. (2012). How is a motor skill learned? Change and invariance at the levels of task success and trajectory control. *Journal of Neurophysiology*, *108*, 578–594.
Shmuelof, L., Yang, J., Caffo, B., Mazzoni, P., & Krakauer, J. W. (2014). The neural correlates of learned motor acuity. *Journal of Neurophysiology*, *112*, 971–980.
Sidarta, A., Vahdat, S., Bernardi, N. F., & Ostry, D. J. (2016). Somatic and reinforcement-based plasticity in the initial stages of human motor learning. *Journal of Neuroscience*, *36*, 11682–11692.
Smith, S. M., Jenkinson, M., Woolrich, M. W., Beckmann, C. F., Behrens, T. E., Johansen-Berg, H., et al. (2004). Advances in functional and structural MR image analysis and implementation as FSL. *Neuroimage*, *23*, S208–S219.
Tootell, R. B. H., Reppas, J. B., Kwong, K. K., Malach, R., Born, R. T., Brady, T. J., et al. (1995). Functional analysis of human MT and related visual cortical areas using magnetic resonance imaging. *Journal of Neuroscience*, *15*, 3215–3230.
Vahdat, S., Darainy, M., Milner, T. E., & Ostry, D. J. (2011). Functionally specific changes in resting-state sensorimotor networks after motor learning. *Journal of Neuroscience*, *31*, 16907–16915.
Voogd, J., Schraa-Tam, C. K. L., van der Geest, J. N., & De Zeeuw, C. I. (2012). Visuomotor cerebellum in human and nonhuman primates. *Cerebellum*, *11*, 392–410.
Wickens, J. R., Reynolds, J. N. J., & Hyland, B. I. (2003). Neural mechanisms of reward-related motor learning. *Current Opinion in Neurobiology*, *13*, 685–690.
Widmer, M., Ziegler, N., Held, J., Luft, A., & Lutz, K. (2016). Rewarding feedback promotes motor skill consolidation via striatal activity. *Progress in Brain Research*, *229*, 303–323.
Wolpert, D. M., Diedrichsen, J., & Flanagan, J. R. (2011). Principles of sensorimotor learning. *Nature Reviews Neuroscience*, *12*, 739–751.
Xiong, G., & Nagao, S. (2002). The lobulus petrosus of the paraflocculus relays cortical visual inputs to the posterior interposed and lateral cerebellar nuclei: An anterograde and retrograde tracing study in the monkey. *Experimental Brain Research*, *147*, 252–263.
Zeki, S. M. (1974). Functional organization of a visual area in the posterior bank of the superior temporal sulcus of the rhesus monkey. *Journal of Physiology*, *236*, 549–573.